ACS APPLIED MATERIALS & INTERFACES

RESEARCH ARTICLE

www.acsami.org

Tunable Luminescence and Energy Transfer properties of $Sr_3AlO_4F:RE^{3+}$ (RE = Tm/Tb, Eu, Ce) Phosphors

Mengmeng Shang,[†,‡] Guogang Li,[†,‡] Xiaojiao Kang,[†,‡] Dongmei Yang,[†,‡] Dongling Geng,[†,‡] and Jun Lin*[,†]

[†]State Key Laboratory of Rare Earth Resource Utilization, Changchun Institute of Applied Chemistry, Chinese Academy of Sciences, Changchun 130022

[‡]Graduate School of the Chinese Academy of Sciences, Beijing 100049, P. R. China

Supporting Information

ABSTRACT: $Sr_3AlO_4F:RE^{3+}$ (RE = Tm/Tb, Eu, Ce) phosphors were prepared by the conventional solid-state reaction. X-ray diffraction (XRD), field-emission scanning electron microscopy (FE-SEM), photoluminescence (PL) spectra, as well as lifetimes were utilized to characterize samples. Under the excitation of UV light, $Sr_3AlO_4F:Tm^{3+}$, $Sr_3AlO_4F:Tb^{3+}$, and $Sr_3AlO_4F:Eu^{3+}$ exhibit the characteristic emissions of Tm^{3+} ($^1D_2 \rightarrow {}^3F_4$, blue), Tb^{3+} ($^5D_4 \rightarrow {}^7F_5$, green), and Eu^{3+} ($^5D_0 \rightarrow {}^7F_2$, red), respectively. By adjusting the doping concentration of Eu^{3+} ions in $Sr_3AlO_4F:0.10Tm^{3+}$, $0.10Tb^{3+}$, zEu^{3+}, a white emission in a single composition was obtained under the excitation of 360 nm, in which an energy transfer from Tb^{3+} to Eu^{3+} was observed. For $Sr_3AlO_4F:Ce^{3+},Tb^{3+}$ samples, the energy transfer from Ce^{3+} to Tb^{3+} is efficient and demonstrated to be a resonant type via a dipole−quadrupole interaction by comparing the experimental data and theoretical calculation. Furthermore, the critical distance of the Ce^{3+} and Tb^{3+} ions has also been calculated to be 9.05 Å. The corresponding luminescence and energy transfer mechanisms have been proposed in detail. These phosphors might be promising for use in near-UV LEDs.

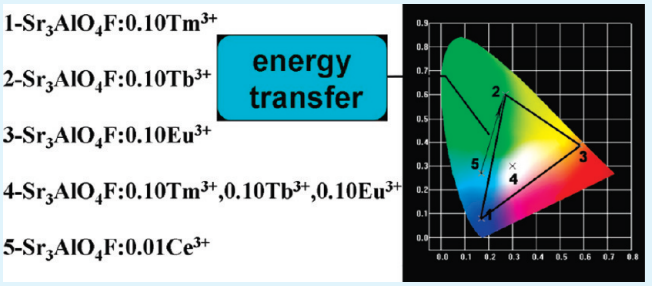

KEYWORDS: Sr_3AlO_4F, rare earth, photoluminescence, white emission, energy transfer

INTRODUCTION

Nowadays the use of inorganic phosphor materials represents a fast growing industry due to the wide range of applications, such as light-emitting diodes (LEDs), cathode ray tubes (CRTs), field-emission displays (FEDs), vacuum fluorescent displays (VFDs), plasma display panels (PDPs), and X-ray imaging scintillators.[1−7] Recently, white light-emitting diodes (LEDs) have received lots of attention in solid-state lighting area because of their advantages such as high energy efficiency, energy savings, and environmental friendliness.[8−12] Nowadays, there are two general approaches to generate white light from LEDs.[13] First, the combination of separate red, green, and blue LEDs creates a white light, which requires complicated electronics and limits its application.[14,15] Second, the white light may be achieved in a very easy and cheap way by combining blue LEDs (460 nm) or UV LEDs (300−410 nm) with phosphors. At present, the combination of blue LEDs with yellow phosphors ($Y_3Al_5O_{12}:Ce^{3+}$) is the most common method to obtain white light. Unfortunately, white light produced by blue LED and yellow phosphors ($Y_3Al_5O_{12}:Ce^{3+}$), possesses poor color-rendering index due to the absence of red light at long wavelength and limits the expansion of the LEDs application.[16,17] Due to this problem, a UV LED (300−410 nm) coated with tricolor phosphors was introduced, which can provide superior color uniformity with a high color rendering index and excellent quality of light.[18] However, the luminescent efficiency is low in this method, which can be attributed to the strong reabsorption.[19,20] In addition, the device of white LEDs with multiple emitting components is very complicated and difficult to be realized. So it is necessary to develop a single-composition white-emitting phosphor which can avoid the above problems. Moreover, it is well-known that the energy transfer plays an important role in luminescent materials both from theoretical and practical points of view.[21] On one hand, it has been recognized that the luminescence intensities of various rare earth ions can be enhanced or quenched by the energy transfer from other codoped rare earth ions; on the other hand, taking into account the application of white LED, the excitation wavelength of some rare ions can not match the requirements for white LED. So some ions such as Gd^{3+}, Eu^{2+}, and Ce^{3+}, whose excitation wavelength usually matches well with the blue- or UV-LED, can be codoped as sensitizers and energy transfer occurs between sensitizers and activators.[22]

Recently, a family of anion ordered oxyfluorides with a general composition $A(1)_{3-x}A(2)_xMO_4F$ [A(1)/A(2) = Sr, Ba, Ca, and

Received: April 30, 2011
Accepted: June 14, 2011
Published: June 14, 2011

M = Al, Ga, In] has aroused great interest and been chosen as host materials for new luminescent materials which can be activated in the deep (200−250 nm) and near (300−400 nm) UV based on their good stability, cheap raw materials, simple synthesis conditions and good luminescence properties.[23−26] However, most of the reports focus on the luminescence properties of Ce^{3+} doped $Sr_{3-x}Ba_xAlO_4F$ for the application in white LED. Here in this manuscript, we synthesized rare earth ions (Tm^{3+}, Tb^{3+}, Eu^{3+}, and/or Ce^{3+}) singly doped or codoped Sr_3AlO_4F phosphors, and investigated their luminescence and energy transfer properties in detail. In general, the different valence states of rare earth ions and Sr^{2+} ion require a charge compensation mechanism. For this reason, the nonstoichiometry of this host lattice ($Sr_{3-3x/2}RE_xAlO_4F$) was performed in actual experiment without adding the charge compensator ions (Li^+, Na^+). In addition, because the experimental techniques we have employed here, namely, X-ray diffraction data and optical properties, are not sensitive to substitutions at this level, we present the formula for the title compounds as written. We find that $Sr_3AlO_4F:Tm^{3+}$ phosphors show blue emission under the excitation of 360 nm, which is suitable for excitation of near-UV LED. More interestingly, by codoping with Tm^{3+}, Tb^{3+}, and Eu^{3+} ions in Sr_3AlO_4F host, we realized white emission in a single composition by adjusting the doping concentration of Eu^{3+} ions. In addition, we codoped Ce^{3+} and Tb^{3+} ions into Sr_3AlO_4F samples in order to make Tb^{3+}-doped Sr_3AlO_4F phosphor with green emission be suitable to UV-LED because Ce^{3+} ions can transfer energy to Tb^{3+} ions under longer UV excitation.

EXPERIMENTAL SECTION

Preparation. Powder samples of Sr_3AlO_4F: RE^{3+} (RE = Tm, Tb, Eu, Ce) were all prepared by a solid-state reaction from $SrCO_3$ (AR), SrF_2 (AR), Al_2O_3 (AR), Tm_2O_3 (99.99%), Tb_4O_7 (99.99%), Eu_2O_3 (99.99%), and $Ce_2(CO_3)_3$ (99.99%). The powder reagents were mixed in an agate mortar by adding ethanol, and then adequately triturated for a good mixing. After being dried in an oven at 80 °C for 20 min, the powder mixtures were then transferred into crucibles and heated at 1200 °C in air for 4 h to produce the final samples.

Characterization. X-ray powder diffraction (XRD) measurements were performed on a D8 Focus diffractometer (Bruker) at a scanning rate of 10°/min in the 2θ range from 20 to 70°, with graphite monochromatized Cu Kα radiation (λ = 0.15405 nm). The morphology of the samples was inspected using a scanning electron microscope (SEM, S-4800, Hitachi). Diffuse reflectance spectra were taken on a Hatachi U-4100 UV−vis−NIR spectrophotometer. The photoluminescence (PL) excitation and emission spectra were recorded with a Hitachi F−7000 spectrophotometer equipped with a 150 W xenon lamp as the excitation source. Luminescence lifetimes were measured with a Lecroy Wave Runner 6100 digital oscilloscope (1 GHz) using a tunable laser (pulse width = 4 ns, gate = 50 ns) as the excitation (Contimuum Sunlite OPO). The absolute quantum efficiencies of the phosphors were determined on a quantum yield measurement system (C9920−02, Hamamatsu Photonics K.K., Japan). All the measurements were performed at room temperature.

RESULTS AND DISCUSSION

Structure and Morphology. The composition, phase purity and morphology of the studied samples were investigated by XRD and FE-SEM. Figure 1A shows the representative XRD patterns for Sr_3AlO_4F, $Sr_3AlO_4F:0.10Tm^{3+}$, $Sr_3AlO_4F:0.10Tb^{3+}$, and $Sr_3AlO_4F:0.10Eu^{3+}$ samples annealed at 1200 °C in air for 4 h, respectively. The diffraction peaks of all these samples can be exactly assigned to the pure tetragonal phase of Sr_3AlO_4F (space group: $I4/mcm$) according to JCPDS file 89−4485. No other phase can be detected, indicating that the RE^{3+} ions are completely dissolved in the Sr_3AlO_4F host. As reported previously,[27,28] the Sr_3AlO_4F host lattice contains two different cation (Sr^{2+}) sites: one [marked as Sr(1)] is located in the layer where the AlO_4 tetrahedra is located and is coordinated by eight oxygen and two apical fluorine; the other one [Sr(2)] is eight coordinated by two fluorines within the $Sr(2)_2F^{3+}$ plane and three oxygen atoms above and three below its plane. Because the coordination environments of the two Sr sites in the compound are noticeably different, it is possible that Sr^{2+} ions ordering can be induced by replacing Sr^{2+} with another alkaline earth ion, or possibly even a rare earth ion and alkali metal cation pair.[29] On

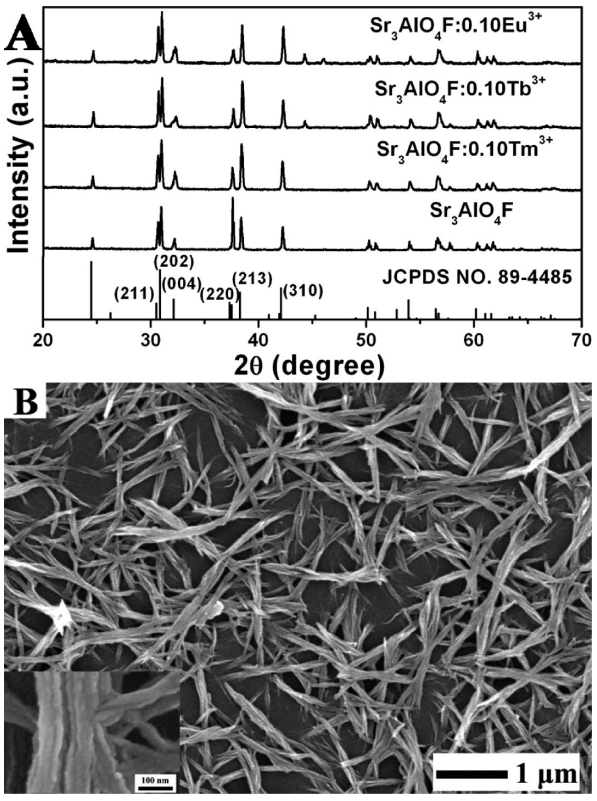

Figure 1. (A) XRD patterns of Sr_3AlO_4F and $Tm^{3+}/Tb^{3+}/Eu^{3+}$-doped Sr_3AlO_4F samples annealed at 1200 °C for 4 h. The standard data for Sr_3AlO_4F (JCPDS 89−4485) are shown as reference; (B) FE-SEM micrograph of the $Sr_3AlO_4F:0.1Tm^{3+}$ sample. The inset is a magnified image.

Table 1. Ionic Radii (Å) of Sr^{2+} and RE^{3+} (RE = Eu, Tb, Tm, Ce) for the Given Coordination Number (CN)

	CN	
	8	10
Sr^{2+}	1.26	1.36
Eu^{3+}	1.07	
Tb^{3+}	1.04	
Tm^{3+}	0.99	
Ce^{3+}	1.14	1.25

the basis of the above analysis and the similar ionic radius between Sr^{2+} and RE^{3+} ions (their ion radii for the given coordination number (CN) are listed in Table 1),[30] the rare earth ions can substitute for Sr^{2+} ions in Sr_3AlO_4F host and therefore, a pure Sr_3AlO_4F phase with no other impurity phase can be obtained.

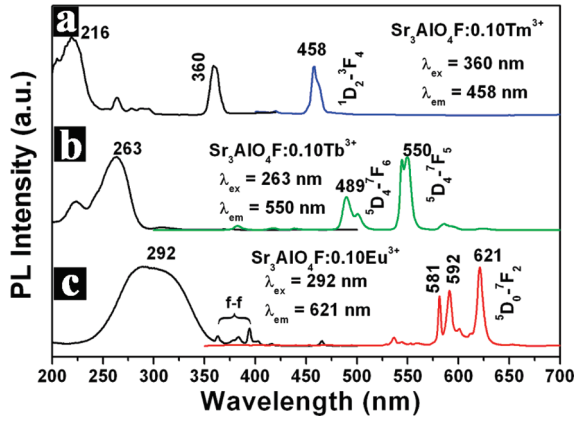

Figure 2. PL excitation (left) and emission (right) spectra of (a) Sr_3AlO_4F: 0.10Tm^{3+}, (b) Sr_3AlO_4F:0.10Tb^{3+}, and (c) Sr_3AlO_4F: 0.10Eu^{3+} samples.

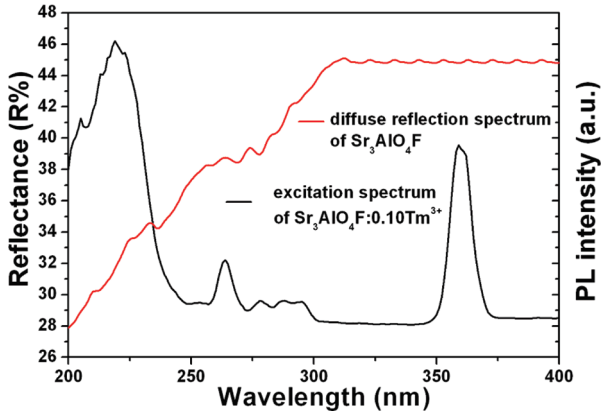

Figure 3. Diffuse reflection spectrum of Sr_3AlO_4F (red line) and the PL excitation spectrum of Sr_3AlO_4F: 0.10Tm^{3+} (black line) for comparison.

Figure 1B shows the FE-SEM micrograph of the Sr_3AlO_4F:0.10Tm^{3+} sample annealed at 1200 °C. At first sight, it seems that the sample is composed of submicrorod bundles with lengths around 1−2 μm and diameters around 200 nm, respectively. A detailed examination of the enlarged FE-SEM micrograph from a selected region (the inset of Figure 1B) indicates that each submicrorod bundle of the sample is the accumulation of nanoparticles. The results for other RE^{3+} ions single-doped or codoped phosphors are similar to that of Sr_3AlO_4F:0.10Tm^{3+} phosphor and will not be shown here.

Photoluminescence Properties of Tm^{3+}, Tb^{3+}, and Eu^{3+}-doped Sr_3AlO_4F. Under UV lamp excitation, Sr_3AlO_4F:Tm^{3+}, Sr_3AlO_4F:Tb^{3+}, and Sr_3AlO_4F:Eu^{3+} samples show bright blue, green, and red luminescence to the naked eye, respectively. The doping concentrations of Tm^{3+}, Tb^{3+}, and Eu^{3+} in Sr_3AlO_4F host have been optimized as 10 at % in our experiments. Figure 2 shows the PL excitation and emission spectra of Sr_3AlO_4F:0.10Tm^{3+}, Sr_3AlO_4F:0.10Tb^{3+}, and Sr_3AlO_4F:0.10Eu^{3+} samples, respectively. The excitation spectrum (Figure 2a) of Sr_3AlO_4F:0.10Tm^{3+} monitored with 458 nm shows two peaks at 360 and 216 nm. The first peak is assigned to the $^3H_6 \rightarrow {}^1D_2$ transition of Tm^{3+} ions.[31] However, the energy of the strong band at 216 nm is higher than $^3P_2$ level of Tm^{3+} at 38193 cm^{-1} (262 nm) and much lower than its $^1S_0$ level at 79592 cm^{-1} (126 nm).[32] So the peak centered at 216 nm was found to be due to absorption of the Sr_3AlO_4F host lattice, which can be confirmed by the diffuse reflection spectrum of Sr_3AlO_4F shown in Figure 3. Upon excitation with 360 nm UV light, the Sr_3AlO_4F: 0.10Tm^{3+} sample shows a blue luminescence with peak at 458 nm, and the corresponding emission spectrum consists of the $^1D_2 \rightarrow {}^3F_4$ transition of Tm^{3+} ions.[21a] For the Sr_3AlO_4F: 0.10Tb^{3+} sample (Figure 2b), the excitation spectrum consists of a strong band at 263 nm and a weak band at 225 nm, which correspond to the spin-allowed (ΔS = 1) and spin-forbidden (ΔS = 0) components of the $4f^8 \rightarrow 4f^7 5d$ transition, respectively.[33] The emission spectrum of Sr_3AlO_4F:0.10Tb^{3+} is dominated by a green emission around 550 nm corresponding to the $^5D_4 \rightarrow {}^7F_5$ transition of Tb^{3+}. Figure 2c shows the PL spectra of Sr_3AlO_4F: 0.10Eu^{3+} sample. The excitation spectrum of

Table 2. Summary of the Photoluminescence Properties of Sr_3AlO_4F: Tm^{3+}, Tb^{3+}, and Eu^{3+} Samples

	excitation peaks (nm)/transition	emission peaks (nm)/transition	quantum yield[a]	CIE color coordinates	color
Tm^{3+}	216/host absorption	458/$^1D_2$−$^3F_4$	2%	x = 0.17	blue
	360/$^3H_6$−$^1D_2$		(360 nm)	y = 0.08	
Tb^{3+}	225(ΔS = 0)/$4f^8$−$4f^7 5d^1$	376/$^5D_3$−$^7F_6$			
	263(ΔS = 1) /$4f^8$−$4f^7 5d^1$	418/$^5D_3$−$^7F_5$	34%	x = 0.27	green
	300−400/4f−4f	440/$^5D_3$−$^7F_4$	(263 nm)	y = 0.60	
		489/$^5D_4$−$^7F_6$			
		550/$^5D_4$−$^7F_5$			
		585/$^5D_4$−$^7F_4$			
		620/$^5D_4$−$^7F_3$			
Eu^{3+}	292/Eu^{3+}−O^{2-} CTB	539/$^5D_1$−$^7F_1$			
	365/$^7F_0$−$^5D_4$	581/$^5D_0$−$^7F_0$	26%	x = 0.58	red
	385/$^7F_0$−$^5G_2$	592/$^5D_0$−$^7F_1$	(292 nm)	y = 0.39	
	397/$^7F_0$−$^5L_6$	621/$^5D_0$−$^7F_2$			
	416/$^7F_0$−$^5D_3$				
	468/$^7F_0$−$^5D_2$				

[a] Quantum efficiency QY refers to the absolute quantum efficiency.

Sr_3AlO_4F:0.10Eu^{3+} can be divided into two parts: one part is from 230 to 350 nm with a maximum at 292 nm, which is attributed to the CTB of O^{2-}—Eu^{3+},[34] the other part from 350 to 500 nm consists of f-f transitions of Eu^{3+} ions. The major red emission peak of Sr_3AlO_4F:0.10Eu^{3+} sample locates at 621 nm together with some weak peaks assigned to the $^5D_1 \rightarrow {}^7F_2$, $^5D_0 \rightarrow {}^7F_0$, $^5D_1 \rightarrow {}^7F_3$, $^5D_0 \rightarrow {}^7F_1$ in the range from 500 to 600 nm. Detailed assignments of Tm^{3+}, Tb^{3+}, and Eu^{3+}-doped Sr_3AlO_4F phosphors for the excitation and emission peaks and luminescent properties, e.g., CIE chromaticity coordinates, lifetimes, absolute quantum yields (QY), and emission colors, are listed in Table 2.

On the basis of the above analyses, it can be clearly known that Tm^{3+}, Tb^{3+}, and Eu^{3+} doped Sr_3AlO_4F samples can be activated with a 360 nm wavelength accessible with near UV-InGaN light-emitting devices. Figure 4 shows the CIE coordinates of Sr_3AlO_4F:Tm^{3+}, Sr_3AlO_4F:Tb^{3+}, and Sr_3AlO_4F:Eu^{3+} samples. Solid-lined triangle depicts the tunable color region of Tm^{3+}, Tb^{3+}, and Eu^{3+} codoped Sr_3AlO_4F. To obtain white light emission in a single component, we codoped Tm^{3+}, Tb^{3+}, and Eu^{3+} ions in Sr_3AlO_4F host. Figure 5 gives the typical PL emission spectra of the representative Sr_3AlO_4F:0.10Tm^{3+}, 0.10Tb^{3+}, zEu^{3+} (z = 0.01, 0.03, 0.05, 0.07, 0.10, 0.30) samples under excitation at 360 nm and the corresponding CIE chromaticity diagram, respectively. Under the excitation of 360 nm, a full-color emission is obtained, resulting from the simultaneous blue, green, and red emission of Tm^{3+}, Tb^{3+}, and Eu^{3+} ions in Sr_3AlO_4F host. As shown in Figure 5, the color tones change from cyan (which is represented at point 1) to cool white (which is represented at point 4), and warm white (points 6) by adjusting the Eu^{3+} doping concentration. Therefore a single-composition white-emitting phosphor is obtained. This white emission is not a function of the excitation. It is obtained by blending simultaneous blue, green, and red emission of Tm^{3+}, Tb^{3+}, and Eu^{3+} ions in Sr_3AlO_4F host. This white emission is dependent on the doping concentration of rare earth ions (Tm^{3+}, Tb^{3+}, and Eu^{3+}). Moreover, it is worthy noting that the luminescent intensity of Tb^{3+} decreases with the increase in Eu^{3+} doping concentrations, whereas the luminescent intensity of Eu^{3+} increases with the increase of Eu^{3+} doping concentrations. The decrease of Tb^{3+} luminescence could be due to an energy transfer from Tb^{3+} to Eu^{3+}. As reported, the luminescence intensities of various rare earth ions can be enhanced or quenched by the energy transfer from other codoped rare earth ions[35] and an energy transfer between Tb^{3+} and Eu^{3+} can occur in some hosts, such as tungstates, zeolite-Y, yttria, porous silicon, borate, hydrate, and molybdates.[36] Additional experimental support on energy transfer from Tb^{3+} to Eu^{3+} came from the lifetime measurements. The decay curves for Sr_3AlO_4F:0.10Tm^{3+}, 0.10Tb^{3+}, zEu^{3+} (z = 0.01, 0.03, 0.05, 0.07, 0.10, 0.30) samples are presented in Figure S1 (see the Supporting Information). The lifetimes are calculated by Origin Program. We transfer the data of decay time directly to Origin Program to get the decay curves, after collecting the data of decay behavior from instrument. These decay curves can be fitted directly and conveniently into double exponential functions in the Origin Program and the lifetime is obtained at the same time. Table 3 gives the lifetimes calculated from Figure S1 in the Supporting Information of Tb^{3+} $^5D_4 \rightarrow {}^7F_5$ transition at 550 nm for different Eu^{3+} concentrations. It can be seen that the lifetime of the Tb^{3+} ions decreases with increasing Eu^{3+} concentration, which strongly supports the energy transfer from the Tb^{3+} to Eu^{3+} ions. The energy transfer efficiency (η_T) from the Tb^{3+} to Eu^{3+} ions in the Sr_3AlO_4F host can be expressed by[37]

$$\eta_T = 1 - \tau_S/\tau_{S0}$$

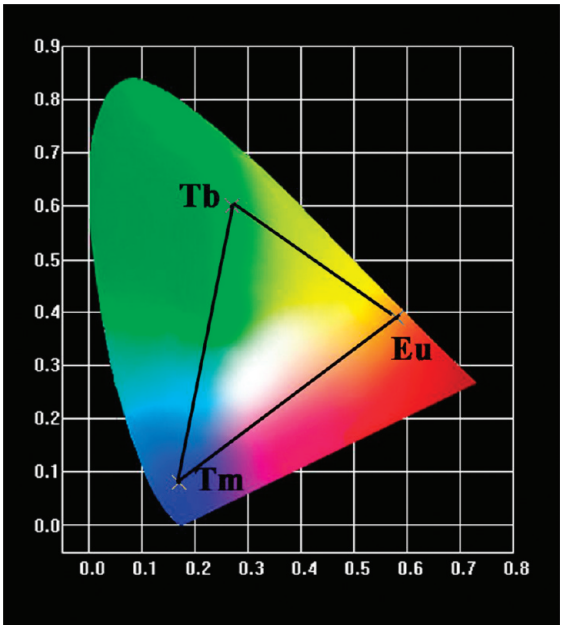

Figure 4. CIE chromaticity diagram for Sr_3AlO_4F: 0.10Tm^{3+}, Sr_3AlO_4F:0.10Tb^{3+}, and Sr_3AlO_4F:0.10Eu^{3+} samples.

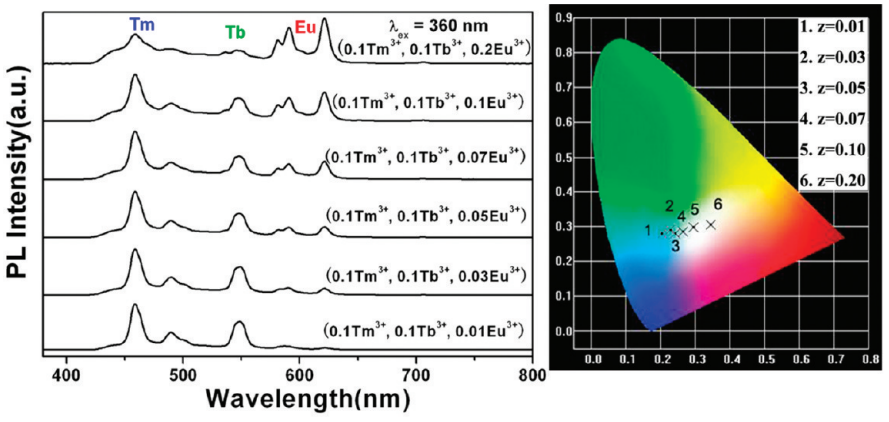

Figure 5. PL emission spectra (left) of Sr_3AlO_4F:0.10Tm^{3+}, 0.10Tb^{3+}, zEu^{3+} samples with different Eu^{3+} concentrations (x = 0.01—0.20). The CIE chromaticity diagram (right) for Sr_3AlO_4F:0.10Tm^{3+}, 0.10Tb^{3+}, zEu^{3+} phosphors: (1) z = 0.01, (2) z = 0.03, (3) z = 0.05, (4) z = 0.07, (5) z = 0.10, (6) z = 0.20.

Table 3. Lifetime τ for the Luminescence of Tb^{3+} ions and Energy Transfer Efficiency (η_T) from Tb^{3+} to Eu^{3+} in the Sr_3AlO_4F:0.10Tm^{3+}, 0.10Tb^{3+}, zEu^{3+} (z = 0−0.20) Samples upon Excitation into the Tb^{3+} with 260 nm

	z						
	0	0.01	0.03	0.05	0.07	0.10	0.20
τ (ms)	2.12	1.36	1.26	1.21	1.19	0.98	0.95
η_T (%)		35.85	40.57	42.92	43.87	53.78	55.19

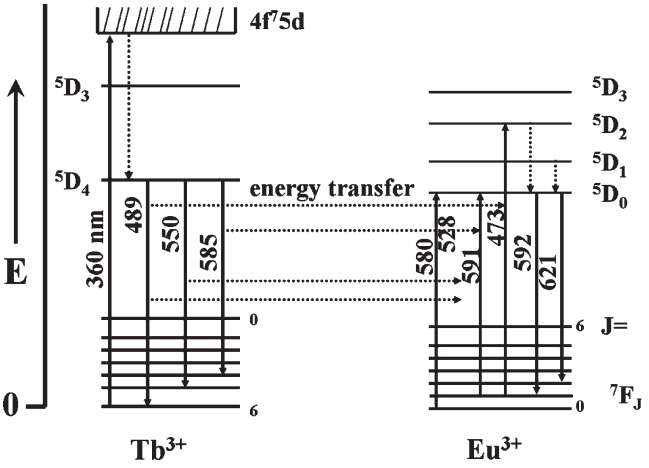

Figure 6. Scheme of energy transfer from Tb^{3+} to Eu^{3+}. The up solid arrows represent photoexcitation, the down solid arrows mean emission, and the down dash arrows denote multiphonon relaxation.

where τ_{S0} and τ_S are the lifetime of the Tb^{3+} in the absence and presence of the Eu^{3+} ions, respectively. The energy transfer efficiency (η_T) from the Tb^{3+} to Eu^{3+} ions in Sr_3AlO_4F host were calculated (Table 3). The energy transfer efficiency η_T increased gradually with increasing Eu^{3+}-doping concentrations. This is because the energy transfer probability from Tb^{3+} to Eu^{3+} is proportional to R^{-6} (R is the average distance between Tb^{3+} and Eu^{3+}).[38] With the increase in Eu^{3+} concentration, average distance (R) between Tb^{3+} and Eu^{3+} is reduced, so the energy transfer efficiency of $Tb^{3+}\rightarrow Eu^{3+}$ is increased. A summary of the emission and energy transfer process of Tb^{3+} and Eu^{3+} in Sr_3AlO_4F host is shown schematically in Figure 6.[36,39] First, electrons on Tb^{3+} ions are excited from the ground state ($4f^8$) to the excited state ($4f^75d$) by 360 nm UV light. Subsequently, these electrons relax to the lowest excited state $^5D_4$ through multiphonon relaxation then either return to the ground state to produce the Tb^{3+} emissions ($^5D_4\rightarrow{}^7F_{6,\,5,\,4}$), or transfer their excitation energy from $^5D_4$ (Tb^{3+}) level to the higher excited energy levels of Eu^{3+} ($4f^6$) through cross relaxation, which relax to the $^5D_0$ (Eu^{3+}) level, where the red-orange emissions ($^5D_0\rightarrow{}^7F_{0,\,1,\,2}$) take place. Because the $^5D_4\rightarrow{}^7F_{6,\,5,\,4,\,3}$ emissions of Tb^{3+} are effectively overlapped with the $^7F_{0,\,1}\rightarrow{}^5D_{0,\,1,\,2}$ absorptions of Eu^{3+}, the energy transfer from Tb^{3+} to Eu^{3+} is very efficient in general.[35b]

Energy Transfer in Sr_3AlO_4F:0.01Ce^{3+}, yTb^{3+} Phosphors. On the basis of the above PL spectra of Sr_3AlO_4F:Tb^{3+} (Figure 2b), only the narrow f-f transition lines (300−500 nm) of Tb^{3+} in the excitation spectrum could be located at the excitation range of near-UV LED. But the f−f absorption

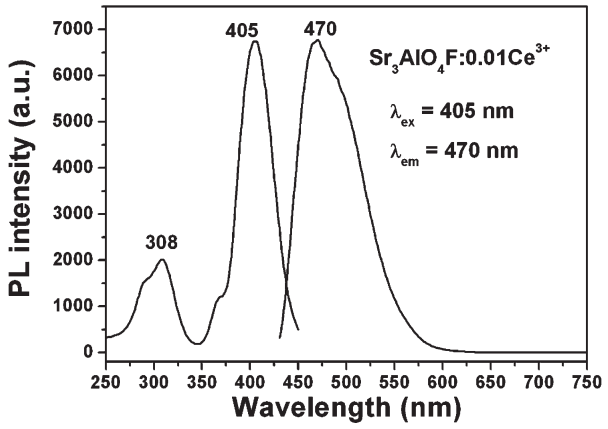

Figure 7. PL excitation and emission spectra of Sr_3AlO_4F:0.01Ce^{3+} sample.

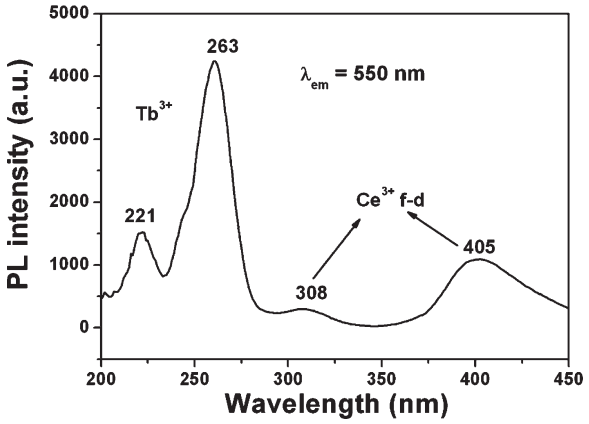

Figure 8. PL excitation spectrum of Sr_3AlO_4F: Ce^{3+}, Tb^{3+} sample monitored at 550 nm.

transitions of Tb^{3+} ions are forbidden transition and therefore, the ions are difficult to pump. In order to overcome this drawback, Ce^{3+} ions can be codoped as sensitizers to transfer excitation energy to Tb^{3+} ions.[40] It has been reported that $Sr_{3-x}A_xAlO_4F$:Ce^{3+} (A = Ba, Ca) phosphors are good luminescent materials for application in LEDs, which is because Ce^{3+} ions in $Sr_{3-x}A_xAlO_4F$ can be efficiently excited by 405 nm and the emission color can be tuned in a large color gamut from blue-green to yellow-green by controlling the Ce^{3+} concentration in Sr_3AlO_4F host.[23,25] It is therefore expected that Tb^{3+} doped Sr_3AlO_4F phosphors can be excited by a near-UV chip and give an intense green emission with the aid of Ce^{3+} ions as sensitizer. For this purpose, we codoped Ce^{3+} and Tb^{3+} ions in Sr_3AlO_4F host to investigate their luminescence properties and energy transfer mechanism in detail. Figure 7 shows the PL excitation and emission spectra of Sr_3AlO_4F:0.01Ce^{3+}. The excitation spectrum shows two bands with maximum at 308 and 405 nm, which are attributed to the electric dipole-allowed transitions of Ce^{3+} ions from the 4f shell to the 5d orbital. Owing to the influences of crystal field splitting and spin−orbit coupling, the 4f→5d transition of Ce^{3+} ions will exhibit a subtle structure. So the excitation spectrum of Ce^{3+} ions shows the direct splitting information of 5d orbital in the crystal field.[41] Under excitation at 405 nm, the emission spectrum of Sr_3AlO_4F:0.01Ce^{3+} exhibits a

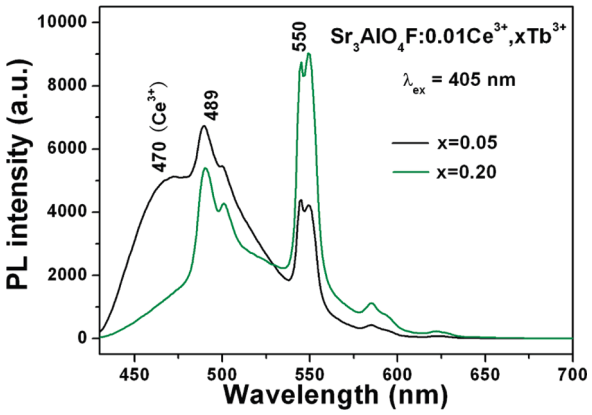

Figure 9. PL emission spectra of representative $Sr_3AlO_4F:0.01Ce^{3+}$, yTb^{3+} (y = 0.05, 0.20) samples under the excitation of 405 nm.

cyan emission band centered at 470 nm, which is assigned to the 5d→4f electronic transition of Ce^{3+} ions. Compared the PL emission of $Sr_3AlO_4F:0.01Ce^{3+}$ (Figure 7) with the PL excitation spectrum of Tb^{3+} (Figure 2b), it can be found that the emission band of the Ce^{3+} ions overlaps with the f-f transition absorptions of Tb^{3+} ions. Therefore, it is expected that a resonance-type energy transfer from Ce^{3+} to Tb^{3+} in $Sr_3AlO_4F:Ce^{3+}$, Tb^{3+} may occur. This can be further confirmed by Figure 8, which shows the PL excitation spectrum of $Sr_3AlO_4F:Ce^{3+}$, Tb^{3+} monitored with the Tb^{3+} emission at 550 nm. It can be observed that except for two broad bands from 200 to 280 nm due to $4f^8 \rightarrow 4f^7 5d$ transition of Tb^{3+} ions, the other two transitions at 308 and 405 nm corresponding to the 4f→5d transition of Ce^{3+} ions are present. To explore the possibility of the energy transfer from the Ce^{3+} to Tb^{3+} ions, Tb^{3+} ions with different concentrations were doped into the $Sr_3AlO_4F:0.01Ce^{3+}$ sample. Figure 9 presents the representative emission spectra of the $Sr_3AlO_4F:0.01Ce^{3+}$, yTb^{3+} samples (y = 0.05 and 0.20). The emission spectra of $Sr_3AlO_4F:0.01Ce^{3+}$, yTb^{3+} consist of both the emission of Ce^{3+} and Tb^{3+} ions and the emission intensity of Ce^{3+} ions decreases with increasing the Tb^{3+} doping concentration, indicating that the energy transfer from the Ce^{3+} to Tb^{3+} ions takes place as expected.

In order to investigate the luminescence dynamics of the samples, we measured the PL decay curves and then calculated the lifetime as well as energy transfer efficiencies, as shown in Figure 10. The decay curves of Ce^{3+} ions can be well fitted to a double-exponential function as $I = A_1\exp(-t/\tau_1) + A_2\exp(-t/\tau_2)$ with a higher goodness fit shown in Figure 10A, which is due to the two different luminescence centers existing in the Sr_3AlO_4F host, as mentioned previously.[23,25,28] The average luminescence lifetimes for Ce^{3+} ions as a function of different Tb^{3+} concentration can be calculated by the formula as $\tau = (A_1\tau_1^2 + A_2\tau_2^2)/(A_1\tau_1 + A_2\tau_2)$, and have been presented in the inset of Figure 10A. It can be seen that the decay lifetime of Ce^{3+} ions decreases with increasing Tb^{3+} concentration, which strongly supports the energy transfer from the Ce^{3+} to Tb^{3+} ions. The energy transfer efficiency (η_T) was calculated by the expression: $\eta_T = 1 - \tau_S/\tau_{S0}$ (where τ_{S0} and τ_S are the lifetime of the Ce^{3+} sensitizer in the absence and presence of Tb^{3+} ions, respectively)[37] and was shown in Figure 10B. The energy transfer efficiency η_T increased with increasing Tb^{3+} doping concentrations.

According to the energy transfer theories of Dexter and Schulman, concentration quenching is due to the energy transfer from one activator to another in many cases until an energy sink

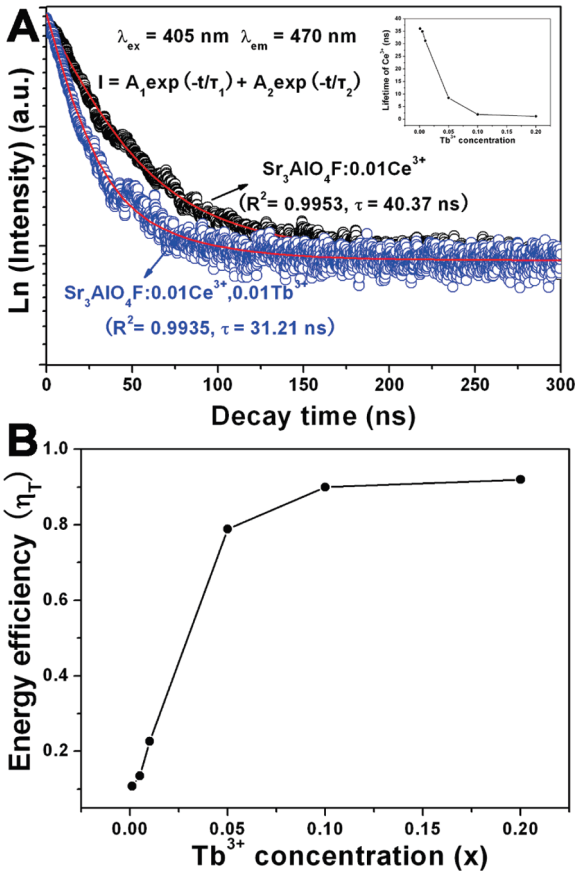

Figure 10. (A) Representative decay curves for the luminescence of Ce^{3+} in Sr_3AlO_4F: $0.01Ce^{3+}$ and $Sr_3AlO_4F:0.01Ce^{3+}$, $0.01Tb^{3+}$; the inset shows the lifetime of Ce^{3+} as a function of Tb^{3+} concentration in $Sr_3AlO_4F:0.01Ce^{3+}$, yTb^{3+}. (B) Dependence of the energy transfer efficiency η_T from Ce^{3+} ions to Tb^{3+} ions in $Sr_3AlO_4F:0.01Ce^{3+}$, yTb^{3+} samples on Tb^{3+} ions doping concentration (y).

in the lattice is reached.[42] As suggested by Blasse,[43] the critical distance R_{Ce-Tb} between Ce^{3+} and Tb^{3+} ions in $Sr_3AlO_4F:0.01Ce^{3+}$, yTb^{3+} samples can be expressed as follows:

$$R_{\text{Ce-Tb}} \approx 2(3V/4\pi\chi_c N)^{1/3} \quad (1)$$

where N is the number of sites that lanthanide ion can occupy in per unit cell, V is the volume of the unit cell, and the critical concentration χ_c is defined as the total doping concentration of Ce^{3+} and Tb^{3+} ions, at which the emission intensity of the Ce^{3+} ions is half that of the sample in the absence of Tb^{3+} ions. For Sr_3AlO_4F host, V = 512.59 Å, N = 12, χ_c = 0.11, and therefore, the critical distance R_{Ce-Tb} of energy transfer was calculated to be 9.05 Å.

On the basis of Dexter's energy transfer expressions of multipolar interaction and Reisfeld's approximation, the following relation can be given as[42,43]

$$\frac{\eta_{S0}}{\eta_S} \propto C^{n/3} \quad (2)$$

where η_{S0} and η_S are the luminescence quantum efficiencies of Ce^{3+} in the absence and presence of Tb^{3+}, respectively; C is the total doping concentration of the Ce^{3+} and Tb^{3+} ions; and n = 6, 8, 10 corresponding to dipole−dipole, dipole−quadrupole, and quadrupole−quadrupole interactions, respectively. The value of

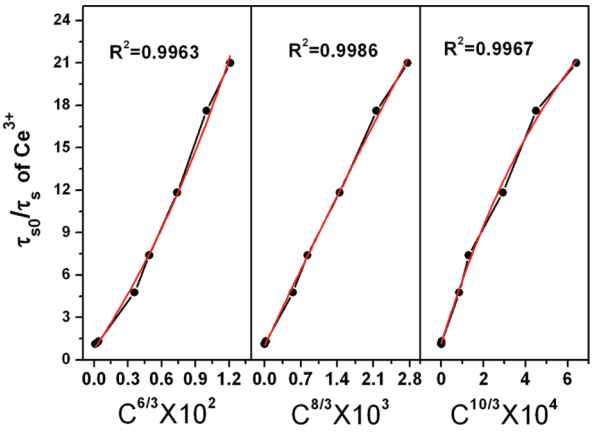

Figure 11. Dependence of τ_{S0}/τ_S of Ce^{3+} ions on $C^{6/3}$, $C^{8/3}$, and $C^{10/3}$.

η_{S0}/η_S can be approximately estimated from the related lifetime's ratio (τ_{S0}/τ_S). So eq 2 can be represented by the following equation

$$\frac{\tau_{S0}}{\tau_S} \propto C^{n/3} \tag{3}$$

The plots of τ_{S0}/τ_S and $C^{n/3}$ are shown in Figure 11. Linear relation is observed only when $n = 8$, implying that the dipole−quadrupole interaction should be mainly responsible for the energy transfer from the Ce^{3+} to Tb^{3+} ions.

According to Dexter's energy transfer theory,[42] the energy transfer process through multipolar interaction depends on the extent of overlap of the emission spectrum of the sensitizer with the absorption spectrum of the activator, the relative orientation of interacting dipoles and the distance between the sensitizer and the activator. For a dipole−dipole interaction, the energy transfer probability (P_{SA}) from a sensitizer to an activator is given by the following formula

$$P_{SA}(dd) = \frac{3 \times 10^{12} f_d}{R^6 \tau_s} \int \frac{fs(E) F_A(E)}{E^4} dE \tag{4}$$

where f_d is the oscillator strength of the involved dipole absorption transition of the activator, τ_S is the radiative decay time of the sensitizer, and R is the sensitizer-activator average distance, $f_S(E)$ represents the normalized emission shape function of the sensitizer and $F_A(E)$ represents the normalized absorption shape function of the activator, and E is the energy involved in the transfer (eV). The critical distance (R_c) of the energy transfer from the sensitizer to activator is defined as the distance for which the probability of transfer equals the probability of radiative emission of the sensitizer, i.e. the distance for which $P_{SA}\tau_S = 1$. Therefore, R_c can be obtained from the formula

$$R_c^6 = 3 \times 10^{12} f_d \int \frac{f_s(E) F_A(E)}{E^4} dE \tag{5}$$

The f_d of the Tb^{3+} transition is 0.3×10^{-6}.[44] Using this value and the calculated spectral overlap, the critical distance for a dipole−dipole interaction mechanism is estimated to be 3.23 Å, which largely deviates from that estimated from the critical concentration data (9.05 Å), further indicating that the electric dipole−dipole interaction can be excluded as the main energy transfer mechanism, which agree with the result obtained by Reisfeld's approximation. Dipole−dipole interactions can generally be expected to dominate in the energy-transfer when both the sensitizer and the activator ions are characterized by an electric dipole-allowed transition, whereas the f−f transitions of the Tb^{3+} ion are forbidden by the selection rules of electric dipole transitions.[45]

For dipole−quadrupole interaction, the energy transfer probability P_{SA} (in s^{-1}) from a sensitizer to an acceptor is given by the following formula[42,43]

$$P_{Ce\text{-}Tb}^{DQ} = 3.024 \times 10^{12} \frac{\lambda_s^2 f_q}{R^8 \tau_s} \int \frac{f_s(E) F_A(E)}{E^4} \tag{6}$$

where f_q is the oscillator strength of the involved absorption transition of the acceptor (Tb^{3+}), λ_S (in Å) is the wavelength position of the sensitizer's emission, τ_S is the radiative decay time of the sensitizer (in seconds), R is the sensitizer−acceptor average distance (in Å), E is the energy involved in the transfer (in eV), andrepresents the spectral overlap between the normalized shapes of the Ce^{3+} emission $f_S(E)$ and the Tb^{3+} excitation $F_A(E)$. The critical distance (R_c) of energy transfer from the sensitizer to the acceptor is defined as the distance for which the probability of transfer equals the probability of radiative emission of donor, the distance for which $P^{DQ}\tau_S = 1$. Hence, R_c can be obtained from eq 6 as

$$R_c^8 = 3.024 \times 10^{12} \lambda_s^2 f_q \int \frac{f_s(E) F_A(E)}{E^4} dE \tag{7}$$

However, the oscillator strength of the Tb^{3+} quadrupole transitions (f_q) did not obtained up to now.[46] It is suggested by Verstegen et al. that the ratio f_q/f_d is about 1×10^{-2} to 1×10^{-3} when f_d applies to a forbidden dipole transition.[44] Using λ_s = 4700 Å, $f_q = 10^{-2}-10^{-3} f_d$, the critical distance (R_c) is obtained to be 11.27−8.45 Å for the dipole−quadrupole interaction, which is consistent with that estimated from the critical concentration data.

In summary, the energy transfer mechanism can briefly described as follows. According the formula: $R_{Ce-Tb} \approx 2(3V/4\pi\chi_c N)^{1/3}$, the R_{Ce-Tb} is calculated to be 9.05 Å. From the model of electric dipole−dipole interaction, R_{Ce-Tb} is calculated to be 3.23 Å. So the model of electric dipole−dipole can be excluded as the main energy transfer mechanism. From the model of dipole−quadrupole interaction, the critical distance is obtained to be 11.27−8.45 Å, which is in consistence with that obtained from the formula: $R_{Ce-Tb} \approx 2(3V/4\pi\chi_c N)^{1/3}$. In addition, dipole−quadrupole interaction as main energy transfer mechanism can also be obtained from the method of Dexter's energy transfer expressions of multipolar interaction and Reisfeld's approximation.[42,43,46]

CONCLUSION

In summary, Tm^{3+}, Tb^{3+}, and/or Eu^{3+}-doped Sr_3AlO_4F phosphors were prepared by a solid-state reaction annealed at 1200 °C for 4 h. Under the excitation of UV light, the Sr_3AlO_4F:Tm^{3+}, Sr_3AlO_4F:Tb^{3+}, and Sr_3AlO_4F:Eu^{3+} phosphors show the characteristic emissions of Tm^{3+} ($^1D_2 \rightarrow {}^3F_4$, blue), Tb^{3+} ($^5D_4 \rightarrow {}^7F_5$, green), and Eu^{3+} ($^5D_0 \rightarrow {}^7F_2$, red), respectively. By codoping Tm^{3+}, Tb^{3+}, Eu^{3+} into Sr_3AlO_4F host, a white light emission in a single phase was obtained under the excitation of 360 nm which is accessible with near UV-InGaN LED. Moreover, in the case of Tm^{3+}-, Tb^{3+}-, Eu^{3+}-codoped systems, energy transfer occurred from Tb^{3+} to Eu^{3+} through multiphonon-assisted process. In Sr_3AlO_4F:Ce^{3+}, Tb^{3+} phosphors, the energy transfer from the Ce^{3+} to Tb^{3+} makes it possible that Sr_3AlO_4F:

Tb^{3+} phosphors can be excited by near UV-LED. By theoretical calculation and comparison, it can be inferred that the energy transfer from Ce^{3+} to Tb^{3+} ions in $Sr_3AlO_4F:Ce^{3+},Tb^{3+}$ phosphors occurs predominantly via the dipole−quadrupole interaction and the critical distance was calculated to be approximately equal to 9.05 Å. Our preliminary studies showed that the Sr_3AlO_4F might be a promising rare earth ions doped host material for application in near-UV LED.

■ ASSOCIATED CONTENT

Supporting Information. Decay curves for the luminescence of Tb^{3+} ions in Sr3AlO4F:0.10Tm^{3+}, 0.10Tb^{3+}, zEu^{3+} samples ($z = 0-0.20$). This material is available free of charge via the Internet at http://pubs.acs.org/.

■ AUTHOR INFORMATION

Corresponding Author
*E-mail: jlin@ciac.jl.cn.

■ ACKNOWLEDGMENT

This project is financially supported by National Basic Research Program of China (2007CB935502, 2010CB327704), and the National Natural Science Foundation of China (NSFC 50872131, 60977013, 20921002).

■ REFERENCES

(1) Rack, P. D.; Naman, A.; Holloway, P. H.; Sun, S. S.; Tuenge, R. T. *MRS Bull.* **1996**, *21*, 49–58.
(2) Piao, X.; Horikawa, T.; Hanzawa, H.; Machidaa, K. *Appl. Phys. Lett.* **2006**, *88*, 161908.
(3) Park, J. K.; Choi, K. J.; Yeon, J. H.; Lee, S. J.; Kim, C. H. *Appl. Phys. Lett.* **2006**, *88*, 043511.
(4) Ko, M. G.; Park, J. C.; Kim, D. K.; Byeon, S. H. *J. Lumin.* **2003**, *104*, 215–221.
(5) Zhou, L.; Choy, W. C. H.; Shi, J.; Gong, M.; Liang, H.; Yuk, T. I. *J. Solid State Chem.* **2005**, *178*, 3004–3009.
(6) Abrams, B. L.; Holloway, P. H. *Chem. Rev.* **2004**, *104*, 5783–5802.
(7) Shea, L. E.; Datta, R. K.; Brown, J. J. *J. Electrochem. Soc.* **1994**, *141*, 2198–2200.
(8) Nakamura, S.; Mukai, T.; Senoh, M. *Appl. Phys. Lett.* **1994**, *64*, 1687.
(9) Pimputkar, S.; Speck, J. S.; DenBaars, S. P.; Nakamura, S. *Nat. Photonics* **2009**, *3*, 180–182.
(10) Schubert, E. F.; Kim, J. K. *Science* **2005**, *308*, 1274–1278.
(11) Hashimoto, T.; Wu, F.; Speck, J. S.; Nakamura, S. *Nat. Mater.* **2007**, *6*, 568–571.
(12) Xie, R. J.; Hirosaki, N.; Mitomo, M.; Sakuma, K.; Kimura, N. *Appl. Phys. Lett.* **2006**, *89*, 241103.
(13) Steigerwald, D. A.; Bhat, J. C.; Collins, D.; Fletcher, R. M.; Holcomb, M. O.; Ludowise, M. J.; Martin, P. S.; Rudaz, S. L. *IEEE J. Sel. Top. Quantum Electron.* **2002**, *8*, 310–320.
(14) Muthu, S.; Schuurmans, F. J. P.; Pashley, M. D. *IEEE J. Sel. Top. Quantum Electron.* **2002**, *8*, 333–338.
(15) Huh, Y. D.; Shim, J. H.; Kim, Y.; Rag Do, Y. *J. Electrochem. Soc.* **2003**, *150*, H57–H60.
(16) Chen, Y.; Gong, M.; Wang, G.; Su, Q. *Appl. Phys. Lett.* **2007**, *91*, 071117.
(17) Jang, H. S.; Im, W. B.; Lee, D. C.; Jeon, D. Y.; Kim, S. S. *J. Lumin.* **2007**, *126*, 371–377.
(18) (a) Shur, M. S.; Zukauskas, A. *Proc. IEEE* **2005**, *93*, 1691–1703. (b) Mueller-Mach, R.; Mueller, G.; Krames, M. R.; Höppe, H. A.; Stadler, F.; Schnick, W.; Jüstel, T.; Schmidt, P. *Phys. Status Solidus A* **2005**, *202*, 1727–1732.(c) Sato, Y.; Takahashi, N.; Sato, S. *Jpn. J. Appl. Phys.* Part 2, **1996**, *35*, L838-L839.
(19) Kido, J.; Shionoya, H.; Nagai, K. *Appl. Phys. Lett.* **1995**, *67*, 2281.
(20) Piao, X. Q.; Horikawa, T.; Hanzawa, H.; Machida, K. *Appl. Phys. Lett.* **2006**, *88*, 161908.
(21) (a) Blasse, G.; Grabmaier, B. C. *Luminescent Materials*; Springer-Verlag: Berlin, 1994; chapters 4−5. (b) Evans, R. C.; Carlos, L. D.; Douglas, P.; Rocha, J. *J. Mater. Chem.* **2008**, *18*, 1100–1107.
(22) (a) Yu, M.; Lin, J.; Zhou, Y. H.; Wang, S. B.; Zhang, H. J. *J. Mater. Chem.* **2002**, *12*, 86–91. (b) Liu, W. R.; Chen, T. M. *J. Phy. Chem. C* **2010**, *114*, 18698–18701. (c) Yang, C. H.; Pan, Y. X.; Zhang, Q. Y. *Mater. Sci. Eng. B—Solid* **2007**, *137*, 195–199.
(23) Chen, W. P.; Liang, H. B.; Ni, H. Y. *J. Electrochem. Soc.* **2010**, *157*, J159–J163.
(24) Park, S.; Vogt, T. *J. Am. Chem. Soc.* **2010**, *132*, 4516–4517.
(25) Bin Im, W.; Brinkley, S.; Hu, J. *Chem. Mater.* **2010**, *22*, 2842–2849.
(26) Park, S.; Vogt, T. *J. Phy. Chem. C* **2010**, *114*, 11576–11583.
(27) Vogt, T.; Woodward, P. M.; Hunter, B. A.; Prodjosantoso, A. K.; Kennedy, B. J. *J. Solid State Chem.* **1999**, *144*, 228–231.
(28) Park, S.; Vogt, T. *J. Lumin.* **2009**, *129*, 952–957.
(29) Prodjosantoso, A. K.; Kennedy, B. J.; Vogt, T.; Woodward, P. M. *J. Solid State Chem.* **2003**, *172*, 89–94.
(30) Su, Q. *Chemistry of Rare Earths*; Henan Science and Technology Press: Zhengzhou, China, 1992; p 8.
(31) Liu, F. S.; Sun, B. J.; Liang, J. K.; Liu, Q. L.; Luo, J.; Zhang, Y.; Wang, L. X.; Yao, J. N.; Rao, G. H. *J. Solid State Chem.* **2005**, *178*, 1064–1070.
(32) Carnall, W. T.; Fields, P. R.; Rajnak, K. *J. Chem. Phys.* **1968**, *49*, 4424–4442.
(33) Li, G. G.; Peng, C.; Zhang, C. M.; Xu, Z. H.; Shang, M. M.; Yang, D. M.; Kang, X. J; Wang, W. X.; Li, C. X.; Cheng, Z. Y.; Lin, J. *Inorg. Chem.* **2010**, *49*, 10522–10535.
(34) Chen, W. P.; Liang, H. B.; Xie, M. B.; Su, Q. *J. Electrochem. Soc.* **2010**, *157*, J21–J24.
(35) (a) Li, G. G.; Li, C. X.; Hou, Z. Y.; Peng, C.; Cheng, Z. Y.; Lin, J. *Opt. Lett.* **2009**, *34*, 3833–3835. (b) Nakazawa, E.; Shionoya, S. *J. Chem. Phys.* **1967**, *47*, 3211–3219. (c) Macedo, A. G.; Ferreira, R. A. S.; Ananias, D.; Reis, M. S.; Amaral, V. S.; Carlos, L. D.; Rocha, J. *Adv. Funct. Mater.* **2010**, *20*, 624–634. (d) Lee, B. H.; Jeong, H. G.; Sohn, K. S. *J. Electrochem. Soc.* **2010**, *157*, J227–J232. (e) Jia, G. H.; Tanner, P. A. *J. Alloys Compd.* **2009**, *471*, 557–560.
(36) (a) Holloway, W. W.; Kestigian, M.; Newman, R. *Phys. Rev. Lett.* **1963**, *11*, 458–460. (b) Chen, W.; Sammynaiken, R.; Huang, Y. *J. Appl. Phys.* **2000**, *88*, 1424–1431. (c) KimAnh, T.; Ngoc, T.; ThuNga, P.; Bitch, V. T.; Long, P.; Strek, W. *J. Lumin.* **1988**, *39*, 215–221. (d) Yang, J.; Zhang, C. M.; Li, C. X.; Yu, Y. N.; Lin, J. *Inorg. Chem.* **2008**, *47*, 7262–7270.
(37) Paulose, P. I.; Jose, G.; Thomas, V.; Unnikrishnan, N. V.; Warrier, M. K. R. *J. Phys. Chem. Solids* **2003**, *64*, 841–846.
(38) Riwotzki, K.; Meyssamy, H.; Kornowski, A.; Haase, M. *J. Phys. Chem. B* **2000**, *104*, 2824–2828.
(39) (a) Moadhen, A.; Elhouichet, H.; Canut, B.; Sandu, C. S.; Oueslati, M.; Roger, J. A. *Mater. Sci. Eng., B* **2003**, *105*, 157–160. (b) Zhang, Z. J.; Chen, H. H.; Yang, X. X.; Zhao, J. T. *Mater. Sci. Eng., B* **2007**, *145*, 34–40. (c) Di, W. H.; Wang, X. J.; Zhu, P. F.; Chen, B. J. *J. Solid State Chem.* **2007**, *180*, 467–473. (d) Kim Anh, T.; Strek, W. *J. Lumin.* **1988**, *42*, 205–210. (e) Schierning, G.; Batentschuk, M.; Osvet, A.; Winnacker, A. *Radiat. Meas.* **2004**, *38*, 529–532.
(40) Zhang, C. M.; Li, C. X.; Peng, C.; Chai, R. T.; Huang, S. S.; Yang, D. M.; Lin, J. *Chem.—Eur. J.* **2010**, *16*, 5672–5680.
(41) Lai, H.; Bao, A.; Yang, Y. M.; Tao, Y. C.; Yang, H.; Zhang, Y.; Han, L. L. *J. Phys. Chem. C* **2008**, *112*, 282–286.
(42) Dexter, D. L. *J. Chem. Phys.* **1953**, *21*, 836–850.
(43) Blasse, G.; Philips *Res. Rep.* **1969**, *24*, 131.
(44) Vestegen, J. M. P. J.; Sommerdijk, J. L.; Verriet, J. G. *J. Lumin.* **1973**, *6*, 425–431.

(45) U Caldiño, G. *J. Phys.: Condens. Matter* **2003**, *15*, 3821–3830.
(46) (a) Huang, Y. J.; You, H. P.; Jia, G.; Song, Y. H.; Zheng, Y. H.; Yang, M.; Liu, K.; Guo, N. *J. Phys. Chem. C* **2010**, *114*, 18051–18058. (b) Zhang, Z.; Wang, J.; Zhang, M.; Zhang, Q.; Su, Q. *Appl. Phys. B:Laser Opt.* **2008**, *91*, 529–537. (c) Huang, C. H.; Kuo, T. W.; Chen, T. M. *ACS Appl. Mater. Interfaces* **2010**, *2*, 1395–1399.